Numerical modelling of a non-Newtonian fluid in the twin-screw pump

Marian Bojko[1,*], *Sylva* Drábková[1], *Josef* Veselý[2], and *Rostislav* Zapletal[2]
[1] VŠB-TU Ostrava, Faculty of Mechanical Engineering, Department of Hydromechanics and Hydraulic Equipment, 17. listopadu 2172/15, Ostrava-Poruba 70800, Czech Republic
[2] Hydrosystem project a. s., tř. Kosmonautů 1103/6a, Hodolany, 77900 Olomouc, Czech Republic

Abstract. Twin screw pump is a positive displacement pump, which is widely used in numerous type of foodstuff applications. Numerical CFD analysis presented in this paper focuses on the investigation of the influence of the clearances and the non-Newtonian behaviour of the fluid. The pump operates at low rotational speed and low inlet pressure. As the first step 3D CFD simulation of twin-screw pump non-rotating segment has been carried out using static mesh without rotation. Various empirical equations have been applied to represent the viscosity relations for non-Newtonian fluid in simple shear. The results are compared for two different values of clearances and various approaches to non-Newtonian fluid description. The obtained results showed the effect of both tested parameters. The physical experiment is under preparation to validate the calculation results.

1 Introduction

Twin screw pump can be classified as the rotary positive displacement pump that displaces a fixed quantity of fluid for every revolution of the driving shaft. The most common arrangement includes two counter rotating screw rotors, one of them is directly connected to the drive and the second is driven by the means of timing gears. Each of the screws comprises two symmetrically opposed screw parts (double suction) with the flow passing from the ends of the screws to the centre of the pump. The scheme of the twin screw pump is presented in Fig. 1.

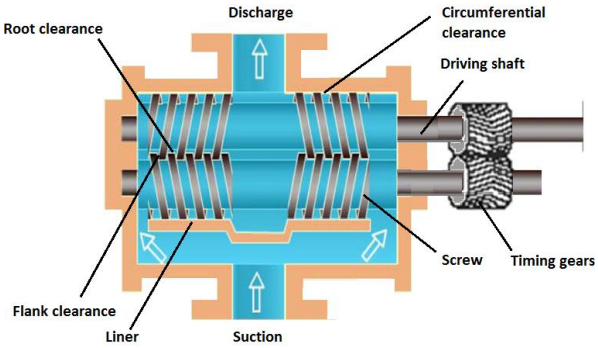

Fig. 1. Scheme of the twin screw pump.

The screws rotate in a liner housing with very small clearances. Figure 1 shows different locations in the pump where clearances occur. We can distinguish the circumferential clearance between screw rotors and liner, the flank clearance between flanks of screw rotors and the root clearance between tip diameter of one screw and root diameter of another screw. These clearances cause an internal leak flow between the discharge higher-pressure and suction lower-pressure sides. The leakage reduces the theoretical (displacement volume) flow rate of the pump and so the volumetric efficiency. In case of highly viscous liquids the leak flow can be assumed laminar and increasing linearly with Δp. The rheological properties of the pumped material have strong influence on screw pump parameters. In case of many food products, the non-Newtonian behaviour must be taken into account.

A lot of research works dealing with the screw pumps have been presented in the field of polymer extrusion. The studies present various approaches to screw extruder design and prediction of its parameters. Differential equations for thermally and hydrodynamically fully developed flow were described in early sixties by Griffith [1]. An analytical model for slightly non-Newtonian biopolymers is presented in [2] and [3]. In recent years the computational fluid dynamics have brought new possibilities to obtain deeper insights in screw pump function and operation. Commercial CFD codes were used first for single screw pump modelling [4]. Development of new grid generation tools have enabled to use the numerical modelling also in case of twin screw pumps with screws intermeshing [5], [6].

The goal of this work was to predict the leakage flow rate first for non-rotating screws. The influence of the clearances and the non-Newtonian behaviour of the fluid was tested on steady screw segments. The laminar flow in internal clearances was investigated for three different geometries of the screws and five rheological functions describing the shear thinning behaviour of the transported material.

* Corresponding author: marian.bojko@vsb.cz

2 Model setup

Model studies have been carried out for non-rotating screw segments with four threads. The design of the screws is conventional, based on constant rotor diameter, pitch and profile shape as depicted in Fig. 2.

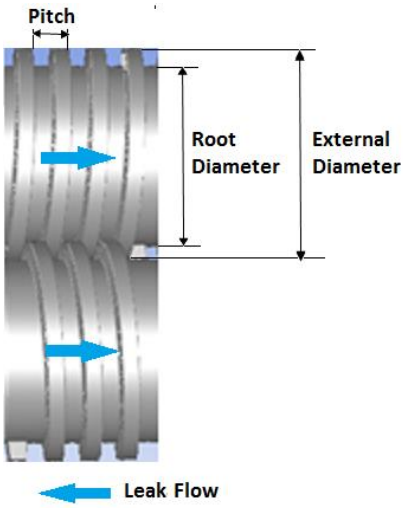

Fig. 2. Screw segments with main dimensions.

The basic geometrical parameters for three variants of screw geometry are defined in Table 1.

Table 1. Geometrical parameters of the screws.

	Geometry version 1:	Geometry version 2:	Geometry version 3:
External diameter (mm)	152	152	159,9
Root diameter (mm)	127	127	119,5
Channel depth (mm)	12,5	12,5	20
Aver. channel width (mm)	12,5	12,5	20
Channel depth (mm)	12,5	12,5	20
Pitch (mm)	25	25	40
Circumferential clearance (mm)	0,7	0,1	0,1
Flank and root clearance (mm)	0,5	0,3	0,3

Inlet and outlet part were connected to the screw segments to enable the definition of boundary conditions as illustrated in Fig. 3.

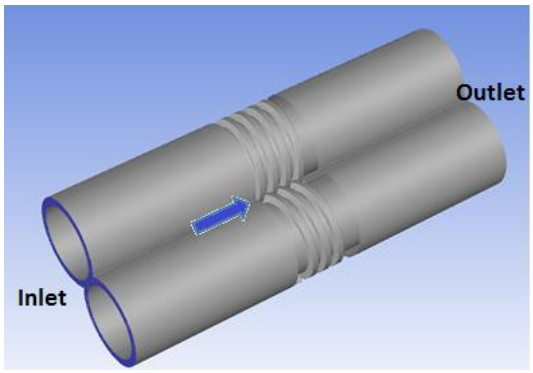

Fig. 3. The modelled geometry with inlet and outlet parts.

3 Non - Newtonian characteristics of the transported material

Tangential shear stress τ is caused by internal friction of the fluid. If the adjacent layers of liquid move at different velocity, their interface shear stress τ arises and it prevents movement. According to Newton's law, this shear stress is linearly proportional to the velocity gradient in the direction perpendicular to the fluid motion.

$$\tau = \eta \frac{du}{dy} \tag{1}$$

where τ is shear stress, du/dy is velocity gradient and η is dynamic viscosity. The ration of tangential shear stress to velocity gradient in Newtonian fluids is constant. For non-Newtonian fluids, this ratio is not constant and different rheological models are defined (for example Power-law model and Herschel-Bulkley model). The Power-law model defines the relationship between the shear stress τ and the shear rate $\gamma=du/dy$ by two parameters, the consistency k and the flow index n in a form:

$$\tau = k\gamma^n \tag{2}$$

The consistency is a constant of proportionality, the flow index defines the degree to which the fluid is shear-thinning. Slightly non-Newtonian materials have a power law index value between 0,7 and 1 and those classified as highly non-Newtonian have values between 0 and 0,7. [3]

The Herschel–Bulkley fluid is generalized, non-linear model of non-Newtonian fluid which combines the Bingham and Power-law fluids in a single relation. Three parameters characterize the relationship between the shear stress τ and the shear rate γ: the consistency k, the flow index n, and the yield shear stress τ_0:

$$\tau = \tau_0 + k\gamma^n \tag{3}$$

The yield stress τ_0 quantifies the amount of stress that the fluid resists before it yields and begins to flow. Applied Power-law functions are presented in Fig. 4 and Herschel–Bulkley characteristics used in simulation are given in Fig. 5.

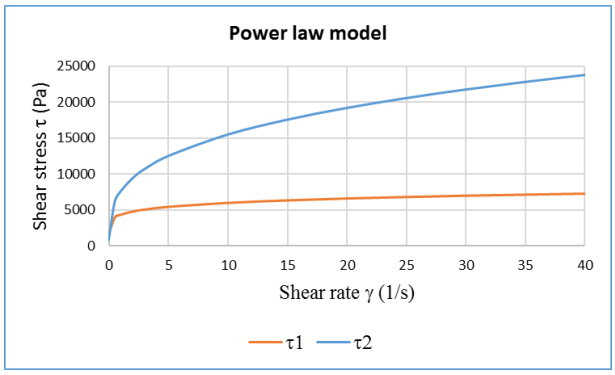

Fig. 4. Power-law characteristics of transported material.

$$\tau_1 = 4295{,}8\gamma^{0{,}1408} \quad (4)$$

$$\tau_2 = 7632{,}6\gamma^{0{,}3081} \quad (5)$$

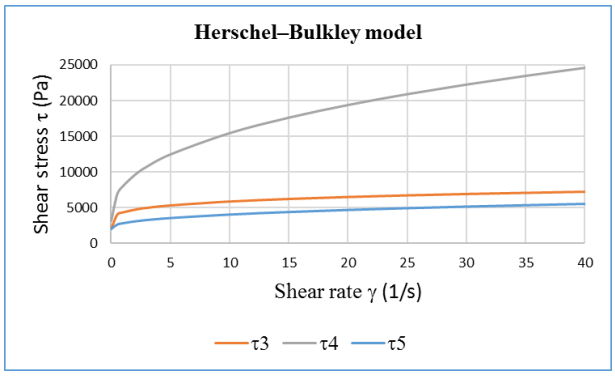

Fig. 5. Herschel–Bulkley characteristics of transported material.

$$\tau_3 = 2050 + 2330\gamma^{0{,}219} \quad (6)$$

$$\tau_4 = 3100 + 4908\gamma^{0{,}401} \quad (7)$$

$$\tau_5 = 1986{,}78 + 823{,}38\gamma^{0{,}3978} \quad (8)$$

4 Mathematical model of fluid flow

The flow of highly viscous substances in the screw pump is characterized as a laminar, stationary flow of incompressible substance in a general three-dimensional region. The resulting mathematical model is defined by basic balance equations such as continuity equations and Navier-Stokes equations for laminar flow [7]:

Mass conservation (continuity equation)

$$\frac{\partial(\rho)}{\partial t} + \nabla \cdot (\rho\vec{u}) = 0 \quad (9)$$

Momentum conservation (Navier- Stokes equation)

$$\frac{\partial(\rho\vec{u})}{\partial t} + \nabla \cdot (\rho\vec{u}\vec{u}) = -\nabla p + [\nabla \cdot \bar{\bar{\tau}}] + \rho\vec{a} + S_m \quad (10)$$

The viscosity of substances is defined by the functional relationships given in chapter 3.

Boundary conditions of the steady isothermal flow computation were the same for each geometry variant and are stated below:

- pressure boundary condition is specified at the inlet ($p = p_i = 3$MPa) and outlet port ($p = p_o = 0.5$MPa),
- no-slip boundary condition is adopted on the stationary walls ($v = 0$).

The geometry of the model and computational grid were prepared in ANSYS DesignModeller [8]. Three variants of geometry were created with different dimensions defined in Table 1. Unstructured computational grid comprises combination of hexagonal, tetrahedral and pyramidal elements. The total number of elements for each geometry variant is presented in Table 2.

Table 2. Number of grid elements

Variant	Number of cells
Geometry variant 1	11 640 331
Geometry variant 2	11 350 618
Geometry variant 3	19 288 383

The grid of the fluid domain is illustrated in Fig. 6.

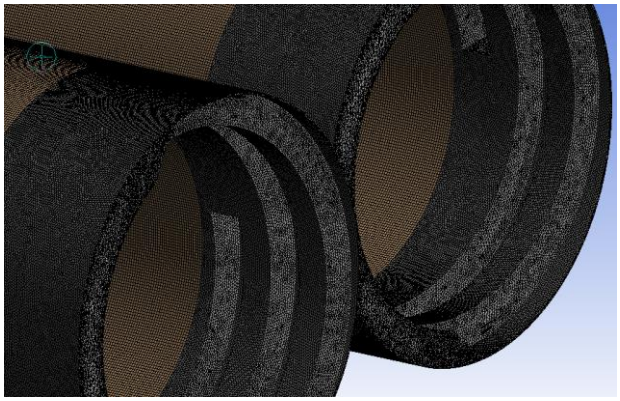

Fig. 6. Grid example of the fluid domain.

The defined mathematical model was applied to three variants of geometry. The same inlet and outlet boundary conditions were defined for each geometry with the objective to evaluate the mass flow-rate for different non-Newtonian fluids defined in chapter 3. Five numerical calculations were performed in ANSYS Fluent for each geometry variant [9].

5 Evaluation of results

The modelling of the flow of non-Newtonian fluids described with function $\tau_1\tau_{,25}\tau_{,4}\tau_{,3}\tau$, was focused on the evaluation of the mass flow- rate for the same pressure drop value of 2.5 MPa. Altogether 15 variants of numerical simulations were realized in ANSYS Fluent environment with the same boundary conditions.

The mass flow-rate predictions from individual CFD analyses are given in Tables 3 and 4 and then compared in the graph (Fig. 7).

Table 3. Calculated mass-flow rate for geometry var.1.

Rheology Description	Geometry variant 1
$\tau_1 = 4295{,}8\gamma^{0{,}1408}$	$Q_{m\text{-}\tau_1}$ = 1760 kg/h
$\tau_2 = 7632{,}6\gamma^{0{,}3081}$	$Q_{m\text{-}\tau_2}$ = 8,87 kg/h
$\tau_3 = 2050 + 2330\gamma^{0{,}219}$	$Q_{m\text{-}\tau_3}$ = 1123 kg/h
$\tau_4 = 3100 + 4908\gamma^{0{,}401}$	$Q_{m\text{-}\tau_4}$ = 10,73 kg/h
$\tau_5 = 1986{,}78 + 823{,}38\gamma^{0{,}3978}$	$Q_{m\text{-}\tau_5}$ =889 kg/h

Table 4. Calculated mass-flow rate for geometry variant 2 and 3**.**

Geometry variant 2	Geometry variant 3
$Q_{m\text{-}\tau_1}$ = 293 kg/h	$Q_{m\text{-}\tau_1}$ = 733,75 kg/h
$Q_{m\text{-}\tau_2}$ = 1,28 kg/h	$Q_{m\text{-}\tau_2}$ = 3,11 kg/h
$Q_{m\text{-}\tau_3}$ = 178 kg/h	$Q_{m\text{-}\tau_3}$ = 480,24 kg/h
$Q_{m\text{-}\tau_4}$ = 1,59 kg/h	$Q_{m\text{-}\tau_4}$ = 3,49 kg/h
$Q_{m\text{-}\tau_5}$ = 109 kg/h	$Q_{m\text{-}\tau_5}$ =271,8 kg/h

Calculated mass-flow rate for three geometry variants and five rheological functions is compared in Figure 7.

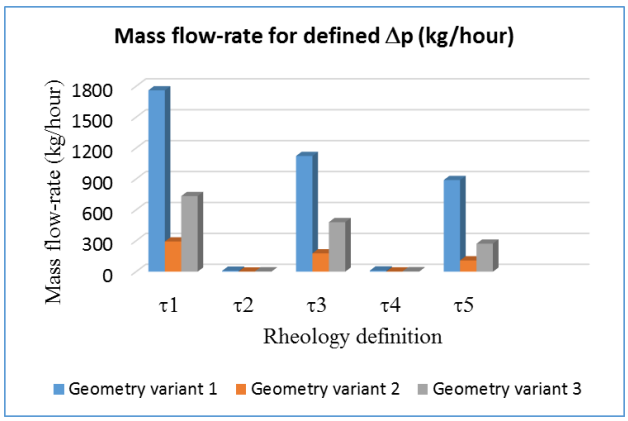

Fig. 7. Comparison of calculated mass flow-rate.

Significantly lower mass flow-rate for non-Newtonian fluid defined by function τ_2 and $_4\tau$ can be observed. The reduction of clearances contributes to leak flow decrease, as can be concluded from comparison of geometry variant 1 and 2 which differ only in clearances.

The example of pressure drop dependent on the length *l* of the modelled geometry variant 1 is evaluated in Fig. 8. The nett pressure drop on the screw segment without inlet and outlet part is given in Table 5.

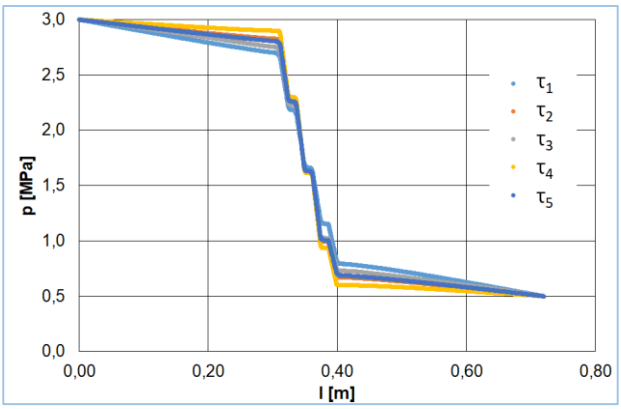

Fig. 8. The pressure drop dependent on the length *l.*

Table 5. The nett pressure drop on the screw segment without inlet and outlet part.

Geometry version 1	Geometry version 2	Geometry version 3
Δp_{τ_1}=1,84 MPa	Δp_{τ_1}=1,99 MPa	Δp_{τ_1}=2,18MPa
Δp_{τ_2}=2,11 MPa	Δp_{τ_2}=2,28 MPa	Δp_{τ_2}=2,37 MPa
Δp_{τ_3}=1,99 MPa	Δp_{τ_3}=2,02 MPa	Δp_{τ_3}=2,2 MPa
Δp_{τ_4}=2,27 MPa	Δp_{τ_4}=2,45 MPa	Δp_{τ_4}=2,48 MPa
Δp_{τ_5}=2,07 MPa	Δp_{τ_5}=2,21 MPa	Δp_{τ_5}=2,33MPa

The pattern of the non-Newtonian fluid flow is evaluated with pathlines colored with velocity magnitude for geometry variants 1 and 2 and rheological function τ_1 and τ_2. It can be observed that the maximum velocity is reached in the narrow gaps between the intermeshing threads of the screws.

The velocity magnitude is corresponding to the value of mass flow-rates given in table 4. In case of τ_1 the flow index *n* is 0,1408 and the mass flow-rate $Q_{m\text{-}\tau_1}$ = 1760 kg/hour for the bigger initial clearances.

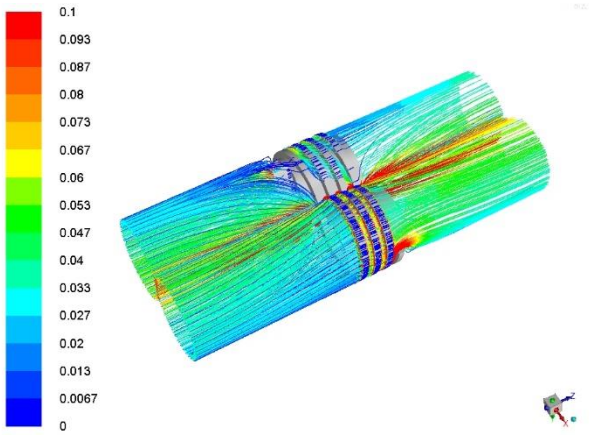

Fig. 9. Pathlines colored by velocity magnitude *u* (range 0 $m{\cdot}s^{-1} \div 0{,}1\ m{\cdot}s^{-1}$) for geometry variant 1 and rheology τ_1.

After reduction of clearances the mass flow-rate decreased to 293 kg/hour and was even more concentrated in the narrow gaps between screw threads.

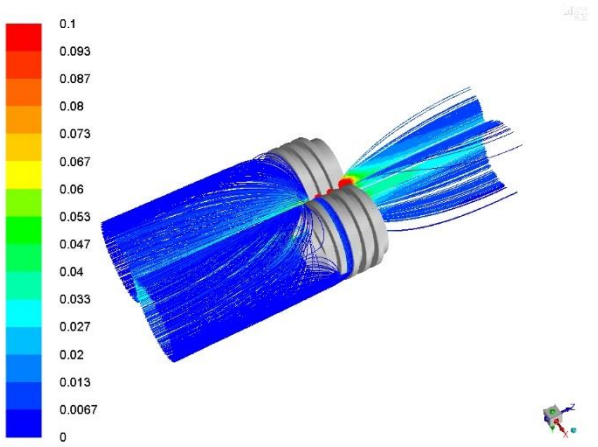

Fig. 10. Pathlines colored by velocity magnitude u (range 0 m·s^{-1} ÷ 0.1 m·s^{-1}) for geometry variant 2 and τ_1.

Similar behaviour can be observed for rheology τ_2 with the flow index n = 0,3081 with mass flow-rate $Q_{m\text{-}\tau_2}$ = 8,87 kg/hour in case of the bigger clearances. After reduction of clearances the mass flow-rate decreased to 1.28 kg/hour and again was concentrated between the screws.

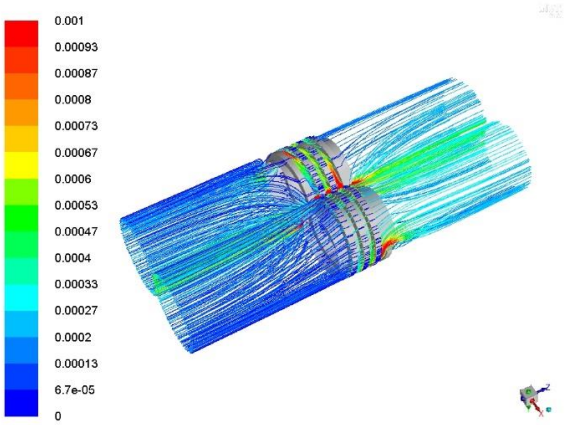

Fig. 11. Pathlines colored by velocity magnitude u (range 0 m·s^{-1} ÷ 0,001 m·s^{-1}) for geometry version 1 and τ_2.

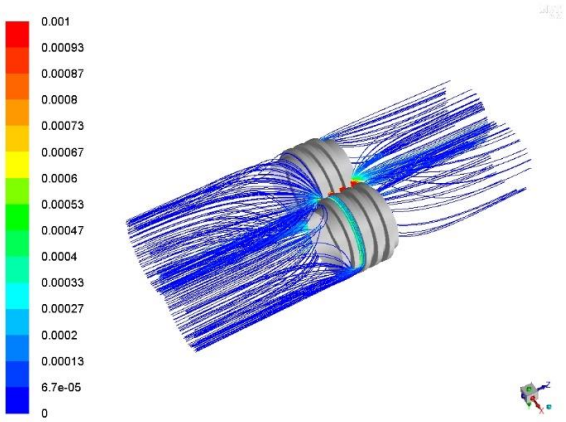

Fig. 12. Pathlines colored by velocity magnitude u (range 0 m·s^{-1} ÷ 0,001 m·s^{-1}) for geometry version 2 and τ_2.

6 Conclusion

This paper deals with the definition of a mathematical model of non-Newtonian fluid flow with different viscosity definitions. Furthermore, the mathematical model is applied to three different geometries of the non-rotating screw segments of the twin screw pump.

The geometry variants 1 and 2 differ only in clearances. The first version of the geometry (Geometry variant 1) has the greatest clearances, and therefore the evaluated mass flow-rate for the same inlet and outlet boundary conditions is significantly higher than for other two geometries in case of all tested rheology functions. The velocity in circumferential clearance between screw rotors and liner is lower than that observed in flank and root clearances. The flow is of similar character as a flow through a straight labyrinth seal [10].

Reduction of clearances leads to decrease of the flow-rate. The geometry variant 3 combines increase of screw channel dimensions with small clearances, which results in higher flow-rates in comparison with variant 2. For comparison of twin screw pump simulation with measurement, the model 1:2 comprising non-rotating screws was prepared and measured. The measured data will be used for validation of results obtained with numerical modelling. The next goal of the work is modelling rotating screws to get more insight of the flow in a twin screw pump.

Acknowledgement

This work was supported by the project Trio FV40105 “Development and production of a prototype of a high-pressure screw pump for pumping highly viscous materials” funded by Ministry of Industry and Trade, Czech Republic.

References

1. R. M. Griffith. Fully Developed Flow in Screw Extruders. Theoretical and Experimental Study. Industrial & Engineering Chemistry Fundamentals 1962 *1* (3), Pages 180-187
2. J. I.Orisaleye, S. J. Ojolo. Parametric analysis and design of straight screw extruder for solids compaction. Journal of King Saud University. Volume 31, Issue 1, January 2019, Pages 86-96
3. J. I. Orisaleye, O. A. Adefuye, A. A. Ogundare, O.L. Fadipe. Parametric analysis and design of a screw extruder for slightly non-Newtonian (pseudoplastic) materials. Engineering Science and Technology. Volume 21, Issue 2, April 2018, Pages 229-237
4. A. Covas, A. Gaspar-Cunha. A computational investigation on the effect of polymer rheology on the performance of a single screw extruder, e-rheo.pt. 1 (2001) 41–62.
5. K. Wilczynski , A. Nastaj, A. Lewandowski, K. J. Wilczynski. Lewandowski, K. Wilczynski. Multipurpose Computer Model for Screw Processing of Plastics. Polymer-Plastics Technology and Engineering. Volume 51, Issue 6, April 2012, Pages 626-633.
6. A. Lewandowski, K. Wilczynski. Computer modeling for polymer processing co-rotating twin screw extrusion – nonconventional screw configurations. Mechanik NR 4/2017.
7. M. Kozubková, T. Blejchař, M. Bojko, Modelování přenosu tepla, hmoty a hybnosti. VŠB-TUO, pp. 174. 2011
8. ANSYS Fluent User's Guide, Release 18.2, 2017 ANSYS, Inc.
9. ANSYS Fluent Theory Guide, Release 18.2, 2017 ANSYS, Inc.
10. M. Kozdera, M. Bojko, S. Drábková, M. Kozubková. Studying the interaction of liquid and solid in the flow of liquid in annulus by CFD analysis. Applied Mechanics and Materials, Volume 630, p. 220-227, 2014.